ENGINE CONTROL SYSTEMS

4.1 Lambda Control

In stoichiometric engine operation, emission levels heavily depend on how accurate the air-fuel ratio can be kept at $\lambda = 1$. Due to measurement and computational tolerances, sufficiently accurate stoichiometric operation requires a closed loop control.

4.1.1 Stochiometric Operation of SI Engines

In SI engines, the air-fuel ratio λ is either very lean at part load or stochiometric at medium and high load. A stoichiometric ratio of $\lambda = 1$ should lead to an ideal combustion. Figure 4.1 shows the emissions at different air-fuel ratios. For $\lambda = 1$, the emissions of HC, CO and NO_x are relatively low. Due to turbulence and local inhomogeneity of the gas mixture, real combustion actually produces HC, CO and NO_x at the same time. By means of a catalytic converter, these raw emissions can be effectively reduced.

It can be seen in Figure 4.2 that the emission rates after the catalytic converter vary highly with the air-fuel ratio λ: A change of the average $\Delta\lambda = 0.1\,\%$ would already double the emission rates. Therefore, it is important to have an accurate closed loop lambda control to guarantee an average air-fuel ratio within a window smaller than $0.1\,\%$ around $\lambda = 1$. When engine speed and torque change, lambda deviations of $2 - 3\,\%$ over a short period of time are allowed. If the average accuracy can be held, such deviations go into both directions. Within the volume of the catalytic converter excursions of the air-fuel ratio in one direction are compensated by those in the opposite direction. At the exhaust pipe tail, short time lambda deviations of a few percent do not deteriorate the emissions after the catalytic converter.

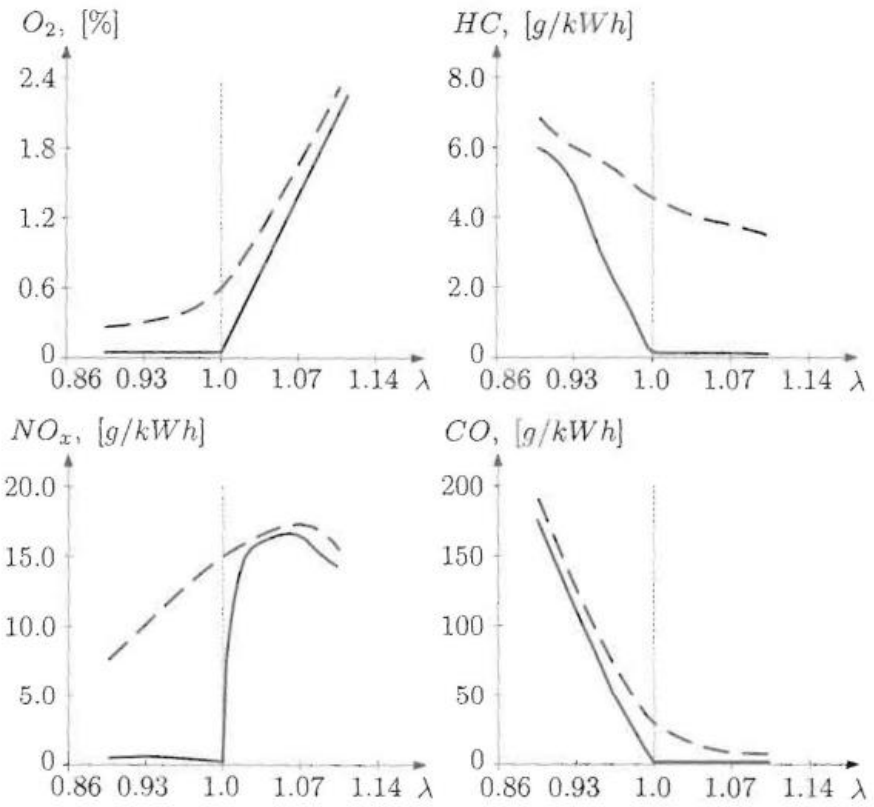

Figure 4.1 Measurement of exhaust gases: oxygen O_2, hydrocarbon HC, nitrogen oxide NO_x and carbon monoxide CO. The concentration before the catalytic converter are indicated by dotted and the concentrations after the catalytic converter by straight lines.

The block diagram of the lambda controlled SI engine is shown in Figure 4.3. The amount of injected fuel is controlled by the engine control unit which gets its feedback from the lambda sensor in the exhaust pipe as well as the mass air flow signal in the inlet pipe. Additional variables like engine speed and engine temperature are also used in the control scheme.

Catalytic Converter

The catalytic aftertreatment reduces the emissions considerably (supposing a correct lambda control at $\lambda = 1$). Due to turbulences and flame propagation, the air-fuel mixture is still uncompletely burned. Noxious gases like HC, CO and NO_x are converted to CO_2, H_2O and N_2 by the catalytic converter. The converter is integrated into the exhaust pipe. It consists of a ceramic or metal carrier substrate covered by a wash coat with an extremely large surface which is again covered with a thin layer of platinum and rhodium as shown in Figure 4.4.

The ratio of platinum to rhodium is approximately 2 to 1. Depending on the engine size about $1 - 3\,g$ of the precious metals are used. They both support

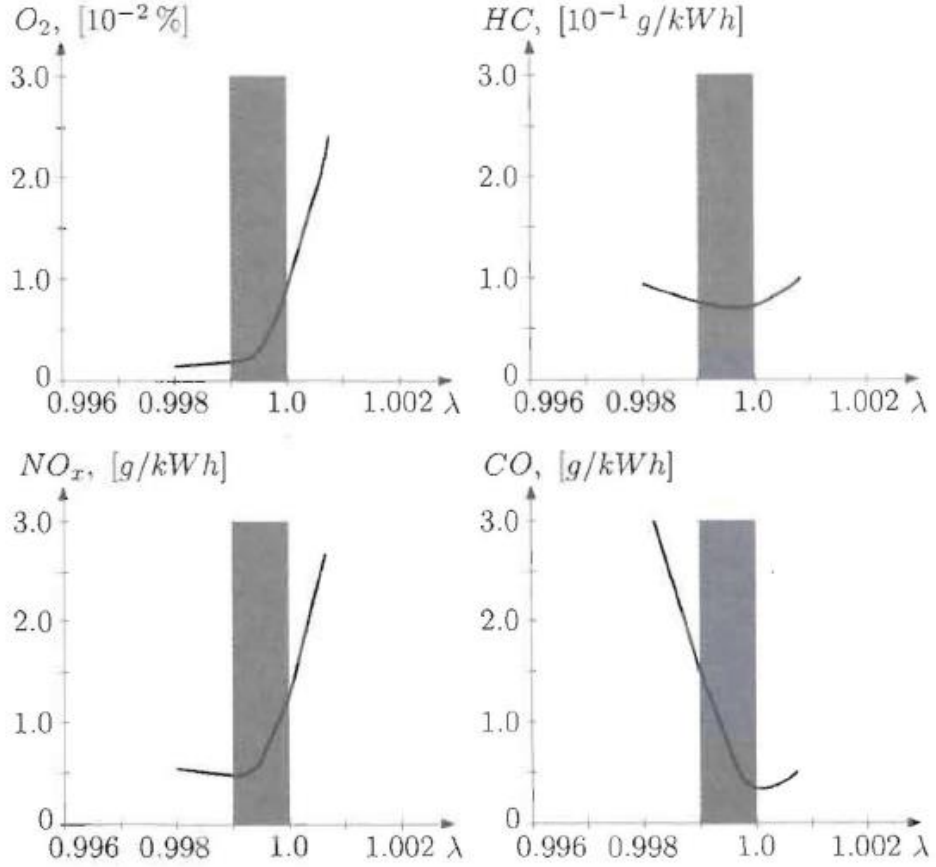

Figure 4.2 Emission rates of an engine after the catalytic converter at a static operating point (engine speed $1800\,rpm$ and torque $T = 65\,Nm$). Average lambda should be within the indicated window.

the chemical reactions: Platin supports more the oxidation of CO and HC and rhodium supports more the reduction of the nitrogen oxides NO_x.

Reduction and oxidation processes are simultaneously running in the catalytic converter. The conversion ratio is defined as the relative change of the gas concentration before and after the catalytic process.

$$c_r = \frac{c_{in} - c_{out}}{c_{in}} \tag{4.1}$$

The conversion ratio has typical values of $c_r > 90\,\%$. The most important chemical reactions are listed below:

Oxidation of HC and CO:

$$H_nC_m + \left(m + \frac{n}{4}\right) O_2 \rightarrow m\,CO_2 + \frac{n}{2} H_2O \tag{4.2}$$

$$H_nC + 2H_2O \rightarrow CO_2 + \left(2 + \frac{n}{2}\right) H_2 \tag{4.3}$$

$$CO + \frac{1}{2} O_2 \rightarrow CO_2 \tag{4.4}$$

$$CO + H_2O \rightarrow CO_2 + H_2 \tag{4.5}$$

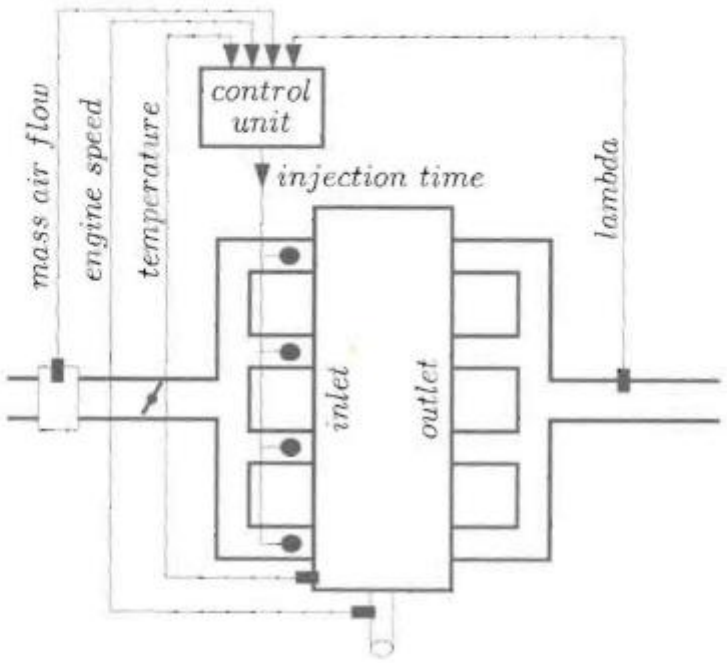

Figure 4.3 Block diagram of a lambda controlled SI engine.

Reduction of NO_x:

$$CO + NO \rightarrow \frac{1}{2}N_2 + CO_2 \tag{4.6}$$

$$H_nC_m + 2\left(m + \frac{n}{4}\right)NO \rightarrow \left(m + \frac{n}{4}\right)N_2 + \frac{n}{2}H_2O + m\,CO_2 \tag{4.7}$$

$$H_2 + NO \rightarrow \frac{1}{2}N_2 + H_2O \tag{4.8}$$

Other catalytic reactions:

$$SO_2 + \frac{1}{2}O_2 \rightarrow SO_3 \tag{4.9}$$

$$SO_2 + 3H_2 \rightarrow H_2S + 2H_2O \tag{4.10}$$

$$\frac{5}{2}H_2 + NO \rightarrow NH_3 + H_2O \tag{4.11}$$

$$2NH_3 + \frac{5}{2}O_2 \rightarrow 2NO + 3H_2O \tag{4.12}$$

$$NH_3 + CH_4 \rightarrow HCN + 3H_2 \tag{4.13}$$

$$H_2 + \frac{1}{2}O_2 \rightarrow H_2O \tag{4.14}$$

The conversion ratio is influenced by the air-fuel ratio and the converter volume. Deviations of $\Delta\lambda < 3\%$ can be compensated for a short period of time. At stationary engine operation, the conversion ratio is high, even if the converter would be already partly damaged. During transients, excursions in the air-fuel

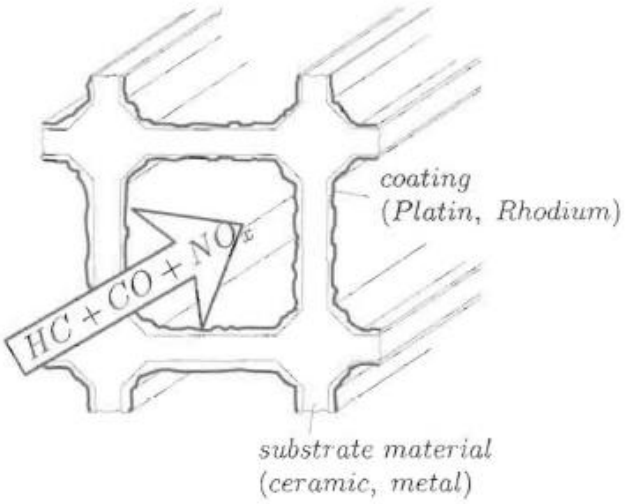

Figure 4.4 Exploded view of a catalytic converter.

ratio occur, leading to higher emissions. During the warm-up phase of the engine and the exhaust pipe, temperatures are too low for chemical reactions and the conversion ratio is poor. The catalytic converter has to reach temperatures beyond $300\,°C$ to be effective. There are several possibilities to accelerate engine warm-up.

- A fast heating of the exhaust pipe can be obtained by an ignition angle retard of e.g. $10° < \Delta\alpha_i < 20°$. The combustion is shifted to a phase of the thermodynamic cycle, where the exhaust valves are already opened.

- An additional start-up catalytic converter is mounted very close to the engine where the exhaust gases get hotter soon. After the warm-up period, this converter is bypassed.

- Fresh air is added to the exhaust gases by a secondary air pump. The engine runs with a rich mixture ($\lambda < 1$). The additional combustion process in the exhaust pipe heats up the catalytic converter.

- The catalytic converter is electrically heated. In order to reduce the required heating power, the heater is concentrated in the region of the converter where the exothermic reaction first starts.

4.1.2 Oxygen Sensor

A lambda sensor is used to measure the concentration of oxygen O_2 in the exhaust pipe. The sensor is mounted in the collective exhaust pipe where the individual exhaust pipes from the cylinders end in. In engines with 6 or more cylinders two lambda sensors are used. In Figure 4.6 it can be seen, that the output voltage increases sharply at $\lambda = 1$. Thus the stochiometric point can be determined.

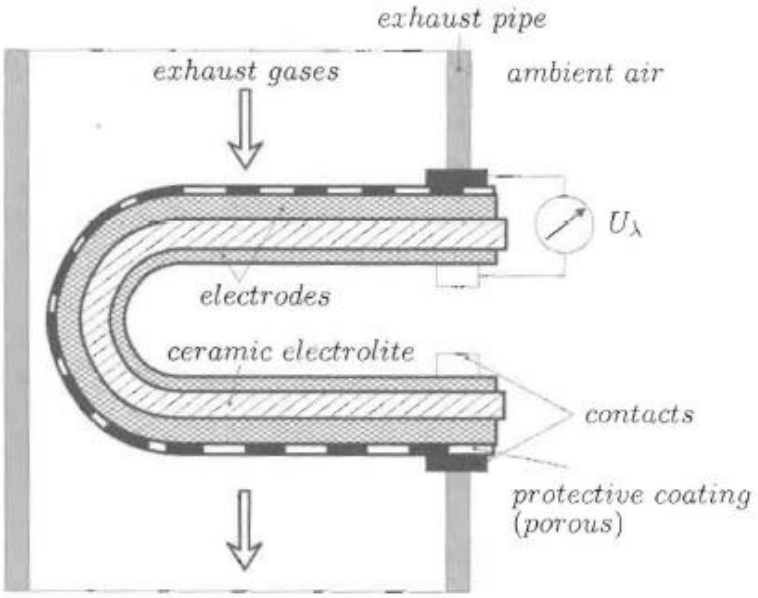

Figure 4.5 Zirconium dioxyde sensor

Zirconium Dioxyde Sensor

The sensor consists of a solid ceramic electrolyte (zirconium dioxyde), which conducts oxygen ions at temperatures above $250\,°C$. The outer electrode is covered with platinum. The oxygen partial pressure on the surface of the ceramic material is thus identical with the one inside the catalytic converter. The inner electrode has a direct contact with the ambient air. The exhaust gases flow around the outer electrodes. Figure 4.5 shows the construction of a Zirconium Dioxyde Sensor.

Because of a difference in the partial oxygen pressure $p(O_2)$ inside and outside of the exhaust pipe, there is an electrolytic voltage between the electrodes:

$$U_\lambda = k\, T_{Sensor}\, ln \frac{p(O_2)_{ambient}}{p(O_2)_{exhaust}} \tag{4.15}$$

The internal resistance ranges from $10^7\,\Omega$ at $200\,°C$ to $5 \cdot 10^3\,\Omega$ at $800\,°C$. Figure 4.6 shows a characteristic step in the sensor voltage curve close to $\lambda = 1$. This step is caused by the increase of the oxygen partial pressure over several orders of magnitude inside the exhaust pipe around $\lambda = 1$. Typical values for the open circuit voltages are:

$$\begin{aligned} U_\lambda(rich) &= 800 - 1000\,mV \\ U_\lambda(lean) &= 50 - 200\,mV \end{aligned}$$

The response time ranges from 15 to $30\,ms$.

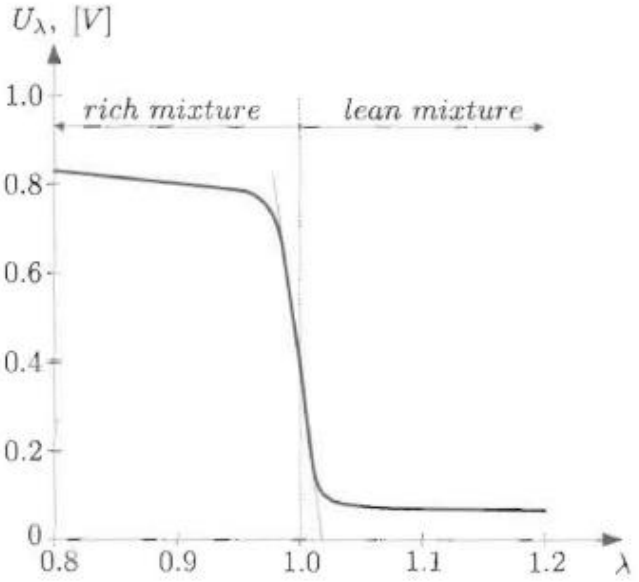

Figure 4.6 Output voltage of zirconium dioxyde sensor

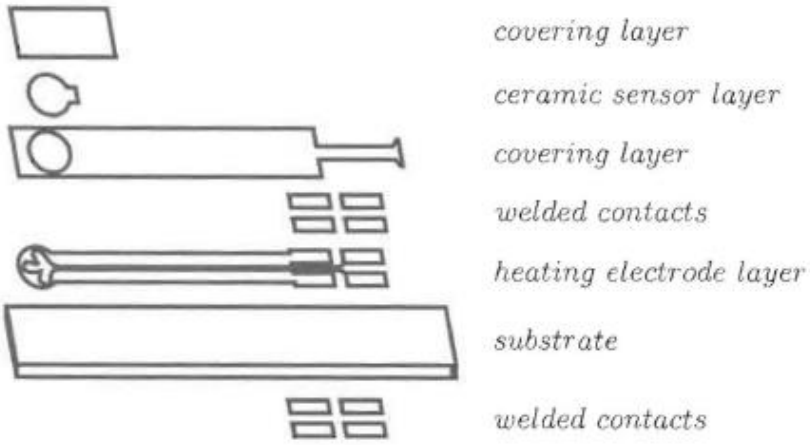

Figure 4.7 Planar structure of the strontium titanate sensor

Strontium Titanate Sensor

Strontium Titanate is a ceramic semiconductor material. Its conductivity depends on the material temperature and oxygen partial pressure. Conductivity in strontium titanate is less influenced by surface effects at high temperatures than in other materials. The dependance of the probe resistance from the temperature decreases at higher temperatures leaving the dependance on lambda only. As can be seen in Figure 4.7, the strontium titanate sensor has a planar structure.

The resistance characteristic of the sensor is shown in Figure 4.8.

An advantage of the planar device is its short response time of a few milliseconds after lambda deviations. The protection pipe around the sensing device adds

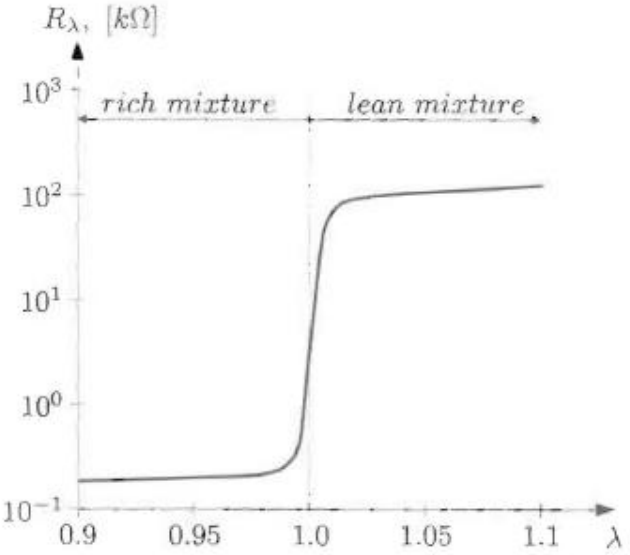

Figure 4.8 Resistance characteristic of the strontium titanate sensor

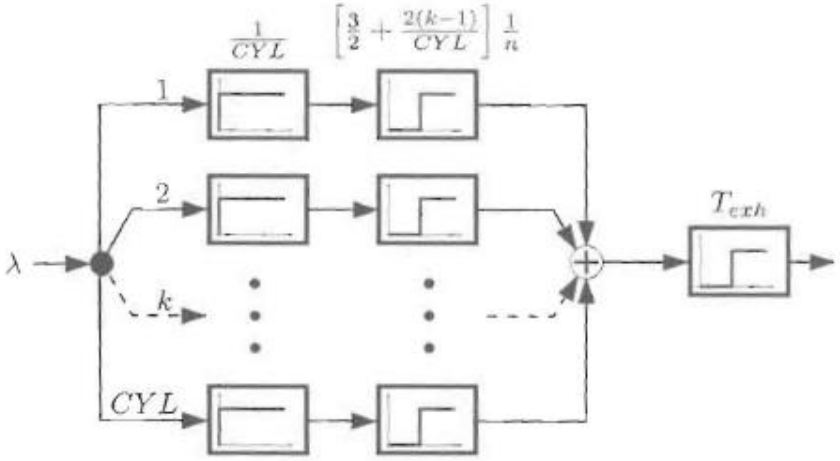

Figure 4.9 Engine model for lambda control

however further delays. Because of its operation at temperatures around 800 °C it can be fitted closer to the engine. In the engine model (see Chapter 4.1.3) this leads to shorter time delays T_{exh} between exhaust valve and lambda sensor.

4.1.3 Engine Model for Lambda Control

Figure 4.9 shows a suitable model of the engine for lambda control,

CYL	is the number of cylinders
k	is the respective cylinder $1, \ldots, CYL$
$\frac{1}{n}$	is the time needed for one crankshaft revolution
T_{exh}	is the time delay between exhaust valve and lambda sensor

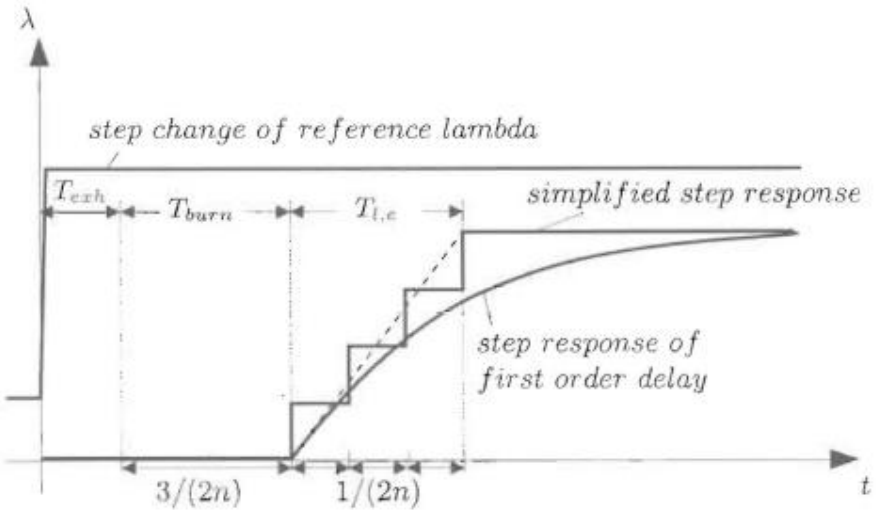

Figure 4.10 Step response and its approximation by a first-order delay (CYL=4)

Its simplified step response can be seen in Figure 4.10.

Fuel is injected into the intake manifold and sucked into the cylinders at phase-shifted time periods. This leads to the stair-step characteristic in the simplified step response. For controller design the steps are approximated by a first-order delay element with the following structure (see also Figure 4.10):

$$\frac{K_{l,e}}{1 + T_{l,e}\, s} \tag{4.16}$$

The combustion can be modeled as dead time T_{burn} continuing until the opening of the exhaust valve. Another dead time T_{exh} results from the time the exhaust gas needs to get to the lambda sensor.

T_{exh}	:	varies in dependence of the mass air flow between 20 and 500 ms
T_{burn}	:	time between opening of inlet and exhaust valves
$T_{l,e}$	:	the approximation delivers $\frac{2(CYL-1)}{n \cdot CYL}$

The dead times can be summed up to:

$$T_{d,e} = T_{exh} + T_{burn}$$

Figure 4.11 shows the simplified engine model containing only one delay time $T_{l,e}$ and only one dead time $T_{d,e}$.

Typical values of the parameters are:

$T_{d,e}$	:	$100\,ms \ldots 1.0\,s$
$T_{l,e}$	:	$50\,ms \ldots 0.5\,s$

Since the model parameters vary significantly with the operating condition of the engine, the parameters of the lambda control are adapted in dependance of

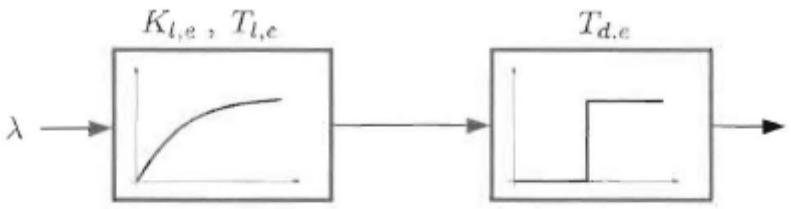

Figure 4.11 Simplified dynamic portion of the engine model

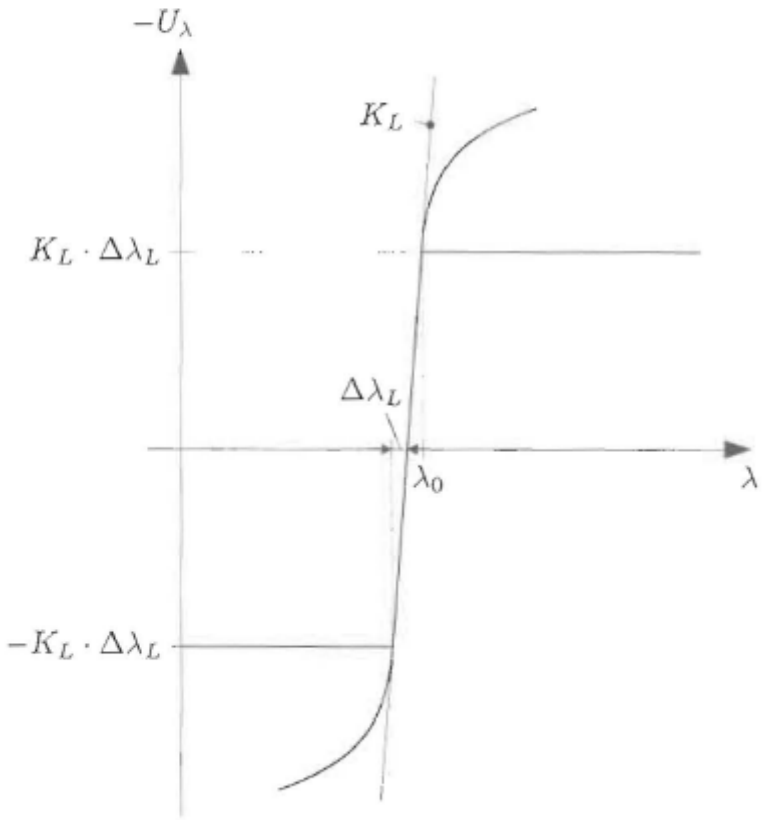

Figure 4.12 Inverted λ-characteristic with limiting range $\pm\Delta\lambda_L$

the engine operating point (feed forward adaption). Each control parameter is stored in a map over the engine's operating points.

4.1.4 Lambda Control Circuit

The characteristic between the output voltage U_λ and the air-fuel ratio λ is non-linear. After operation for many years this characteristic slightly ages. Therefore the most stable measuring range of the characteristic is taken for the control. Figure 4.12 shows, that it is located in the steep linear range of the characteristic. The sensitivity factor in this range is K_L.

Outside the measurement range the characteristic is cut off. The center of the

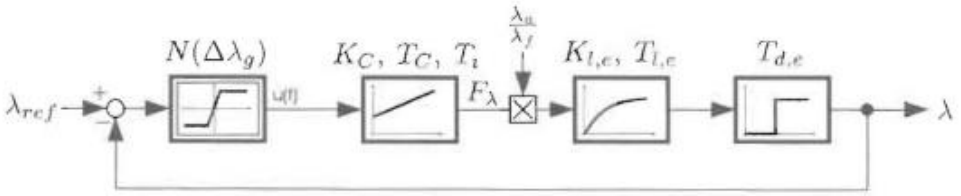

Figure 4.13 Closed loop-control circuit of the lambda-control

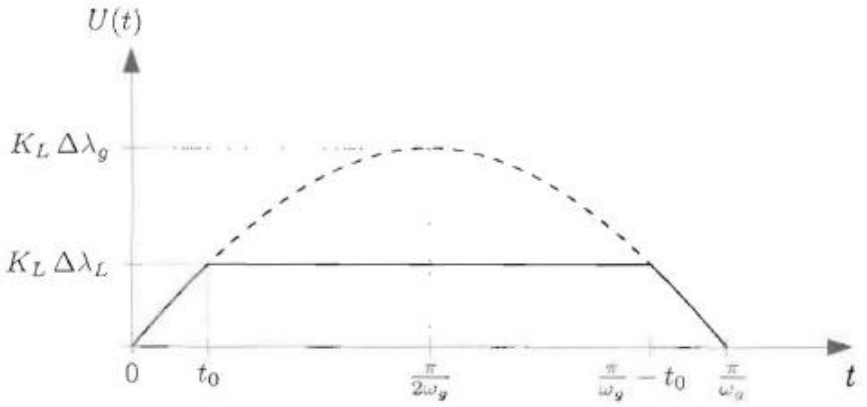

Figure 4.14 Limiting of the output sine function $U(t)$

measurement range λ_0 is not at the desired reference value λ_{ref} but is determined exclusively by the stability of the characteristic. The lambda reference value λ_{ref} must however lie within the range $[\lambda_0 - \Delta\lambda_L, \lambda_0 + \Delta\lambda_L]$. The offset of λ_0 against the reference value λ_{ref} can be compensated e.g. by a direction-dependant integral time constant of the PI controller.

To get the classical structure of a control loop, the sign of the characteristic voltage $U_\lambda(\lambda)$ is inverted. At the input of the controller a non-linear function is doing the range cut-off.

The closed loop-control circuit comprises a non-linear element and a dead time. Therefore it performs a limit cycle. For an analytic calculation the method of the harmonic balance [22] is used where the input of the non-linear element receives a sine function with the limit cycle $\Delta\lambda_g$:

$$\lambda(t) = \Delta\lambda_g \cdot \sin(\omega_g t) \tag{4.17}$$

From the output signal $U(t)$ only the first term $U_1(t)$ of a Fourier expansion is taken. The amplitude of $U_1(t)$ equals the Fourier coefficient U_1 (see Figure 4.14).

$$U_1 = \frac{4\omega_g}{\pi} K_L \left(\int_0^{t_0} \Delta\lambda_g \sin^2(\omega_g t)\, dt + \int_{t_0}^{\frac{\pi}{2\omega_g}} \Delta\lambda_L \sin(\omega_g t)\, dt \right)$$

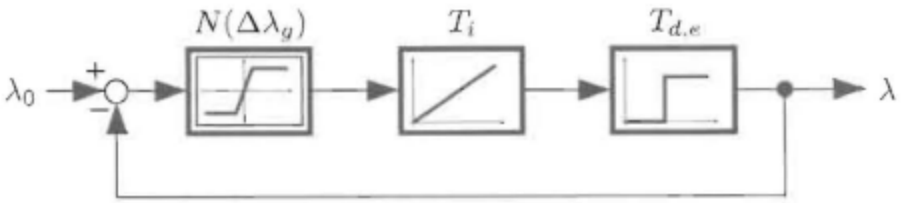

Figure 4.15 Control loop after delay compensation

The time t_0 is given by the ratio of $\Delta\lambda_L$ to $\Delta\lambda_g$:

$$t_0 = \frac{1}{\omega_g} \arcsin\left(\frac{\Delta\lambda_L}{\Delta\lambda_g}\right)$$

Solving the integral and dividing by $\Delta\lambda_g$ leads to the gain $N(\Delta\lambda_g)$ of the non-linear element for the first Fourier term:

$$N(\Delta\lambda_g) = \frac{U_1}{\Delta\lambda_g} = \frac{2}{\pi} K_L \left(\arcsin\left(\frac{\Delta\lambda_L}{\Delta\lambda_g}\right) + \frac{\Delta\lambda_L}{\Delta\lambda_g} \sqrt{1 - \left(\frac{\Delta\lambda_L}{\Delta\lambda_g}\right)^2} \right)$$

If the output range is strongly limited, meaning $\Delta\lambda_L \ll \Delta\lambda_g$, the gain can be approximated by:

$$N(\Delta\lambda_g) \approx \frac{4}{\pi} \left(\frac{\Delta\lambda_L}{\Delta\lambda_g}\right) K_L \tag{4.18}$$

We assume the controller to be a PI-element with the following structure:

$$\frac{1 + T_C\, s}{T_i\, s} \cdot \frac{1}{K_C} \tag{4.19}$$

$$T_C \approx T_{l,e} \tag{4.20}$$

Because $T_{l,e}$ depends strongly on the operation point of the engine, T_C needs to be adapted. Figure 4.15 shows the resulting structure of the control loop after compensation. The open-loop transfer function results to

$$G(s) = N(\Delta\lambda_g) \frac{1}{s\, T_i} \frac{1}{K_C} \cdot e^{-T_{d,e} s} \quad , \tag{4.21}$$

and the open-loop frequency response to

$$G(j\omega) = N(\Delta\lambda_g) \frac{1}{j\omega T_i} \frac{1}{K_C} \cdot \left[\cos\left(\omega T_{d,e}\right) - j \sin\left(\omega T_{d,e}\right)\right] \quad . \tag{4.22}$$

The stability limit of the closed-loop system is at

$$G(j\omega) = -1 \quad . \tag{4.23}$$

The frequency of the limit cycle ω_g results from the imaginary part of $G(j\omega)$:

$$Im\{G(j\omega_g)\} = 0 \qquad \Rightarrow \qquad \cos(\omega_g T_{d,e}) = 0 \tag{4.24}$$

$$\Rightarrow \qquad \omega_g = \frac{\pi}{2 \cdot T_{d,e}} \tag{4.25}$$

With $\omega_g = \frac{\pi}{2 \cdot T_{d,e}}$ the real part yields:

$$Re\{G(j\omega_g)\} = -N(\Delta\lambda_g)\frac{2}{\pi}\frac{1}{K_C}\frac{T_{d,e}}{T_i} \tag{4.26}$$

The stability criterion of the control loop is given by (Figure 4.16):

$$|Re\{G(j\omega_g)\}| \leq 1 \tag{4.27}$$

Inserting Equation 4.26 into Equation 4.27 leads to

$$T_i > N(\Delta\lambda_g)\frac{2}{\pi}\frac{1}{K_C}T_{d,e} \tag{4.28}$$

or with Equation 4.18

$$T_i > \frac{8}{\pi^2} \cdot \frac{\Delta\lambda_L}{\Delta\lambda_g} \cdot \frac{K_L}{K_C} \cdot T_{d,e} \quad . \tag{4.29}$$

The dependence of the parameter $T_{d,e}$ on the operating point of the engine leads to a controlled adaption of the parameter T_i. The maximum amplitude of the limit cycle has been constrained by the lambda-window to:

$$\frac{\Delta\lambda_g}{\lambda} \leq 3\,\% \tag{4.30}$$

This equation determines the minimum value of the integration parameter T_i. Consequently the control loop reacts relatively slow to dynamic transitions between operating points (see also Figure 4.20). During long transient times noxious emissions can no longer be reduced by the catalytic converter.

4.1.5 Measurement Results

If we assume the volume of the catalytic converter to be around $V_C \approx 0.016\,m^3$, then it contains about $m_a = 0.02\,kg$ of air (and noxious exhaust gases). At full engine load and speed, a mass air flow of $\dot{m}_a = 600\,kg/h$ shall run through the exhaust pipe. It will stay $t_C = m_a/\dot{m}_a \approx 120\,ms$ in the catalytic converter. At engine idling, mass air flow might be at $6\,kg/s$. This would stay $t_C \approx 12\,s$ in the converter. The frequency of the lambda control limit cycle must therefore be above

- $0.1\,Hz$ at idling,
- $10\,Hz$ at full load and speed.

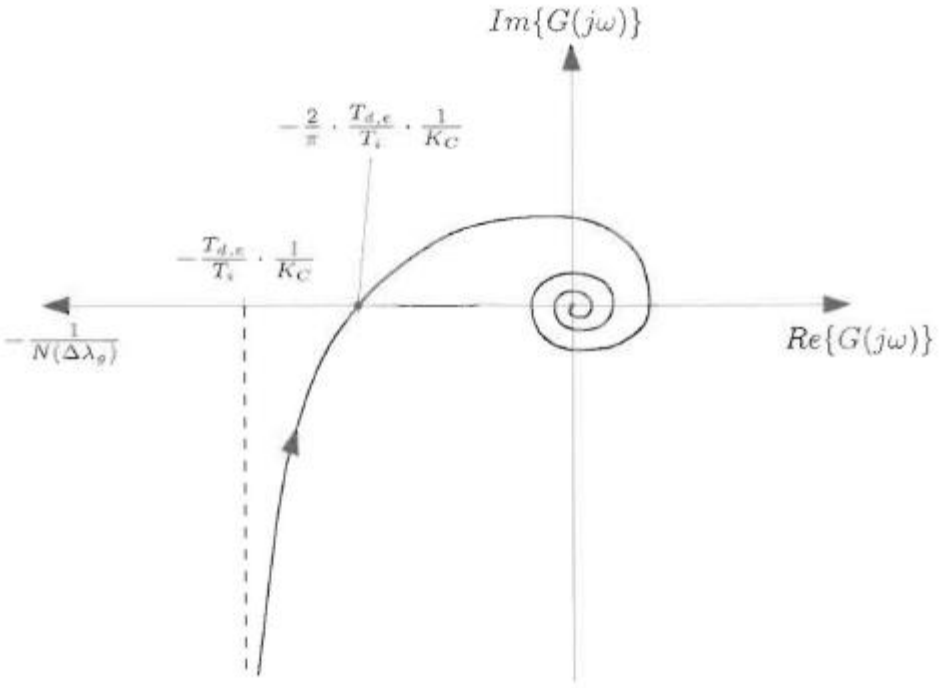

Figure 4.16 Root locus diagram of lambda-control

Figure 4.17 shows measurement results of the lambda control F_λ at an approximately stationary operating point of the engine. Noxious emissions and λ before and after catalytic treatment are shown in one diagramm. At stationary engine operation the catalytic converter has a high conversion ratio.

Figure 4.18 and 4.19 show measurement results of the lambda control during dynamic engine transients of a driving test cycle. Rotational speed and load vary a lot during acceleration and deceleration. At dynamic engine transients we observe fast rotational speed variations e.g. caused by gear changes. Since the integration time constant is limited by the lambda control limit cycle amplitude, mismatches occur where the lambda window is left and high peaks of noxious emissions are generated.

4.1.6 Adaptive Lambda Control

The dynamic performance of the lambda control is strongly restricted by the following parameters:

- given dead time of the engine $T_{d,e}$ (see Chapter 4.1.3)
- amplitude of limit cycle $\Delta\lambda_g$ limited at short-time deviations $< 3\,\%$ (see Equation 4.30)

The integration time constant T_i of the controller is constrained to the lower limit given in Equation 4.29. At engine transients to another operating point, the lambda control needs up to several seconds for arriving back to the stochiometric mixture (see Figure 4.20).

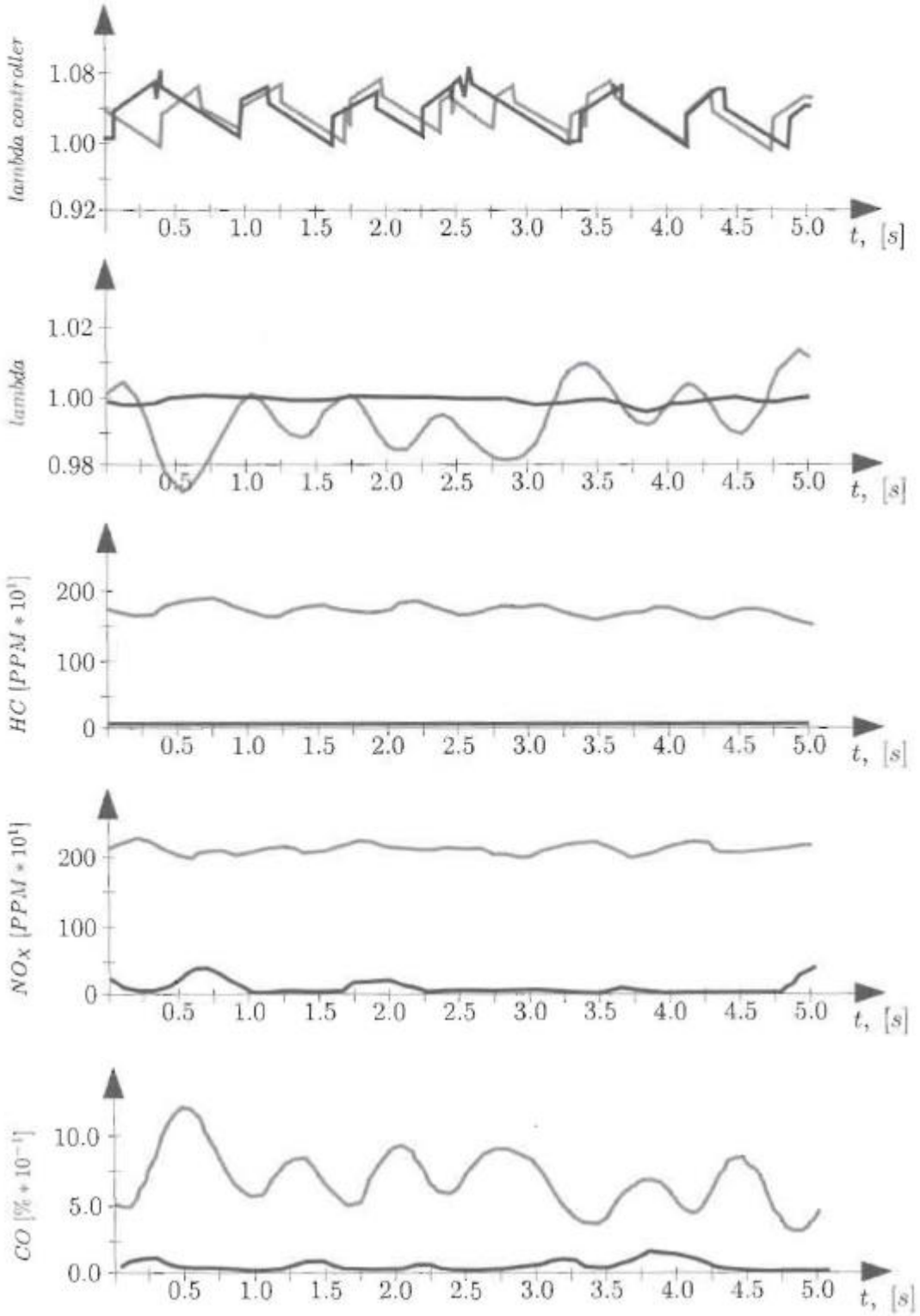

Figure 4.17 Emissions of lambda-controlled engine at stationary engine operation with $n = 1800/min$, $T = 65\,Nm$, before and after catalytic converter

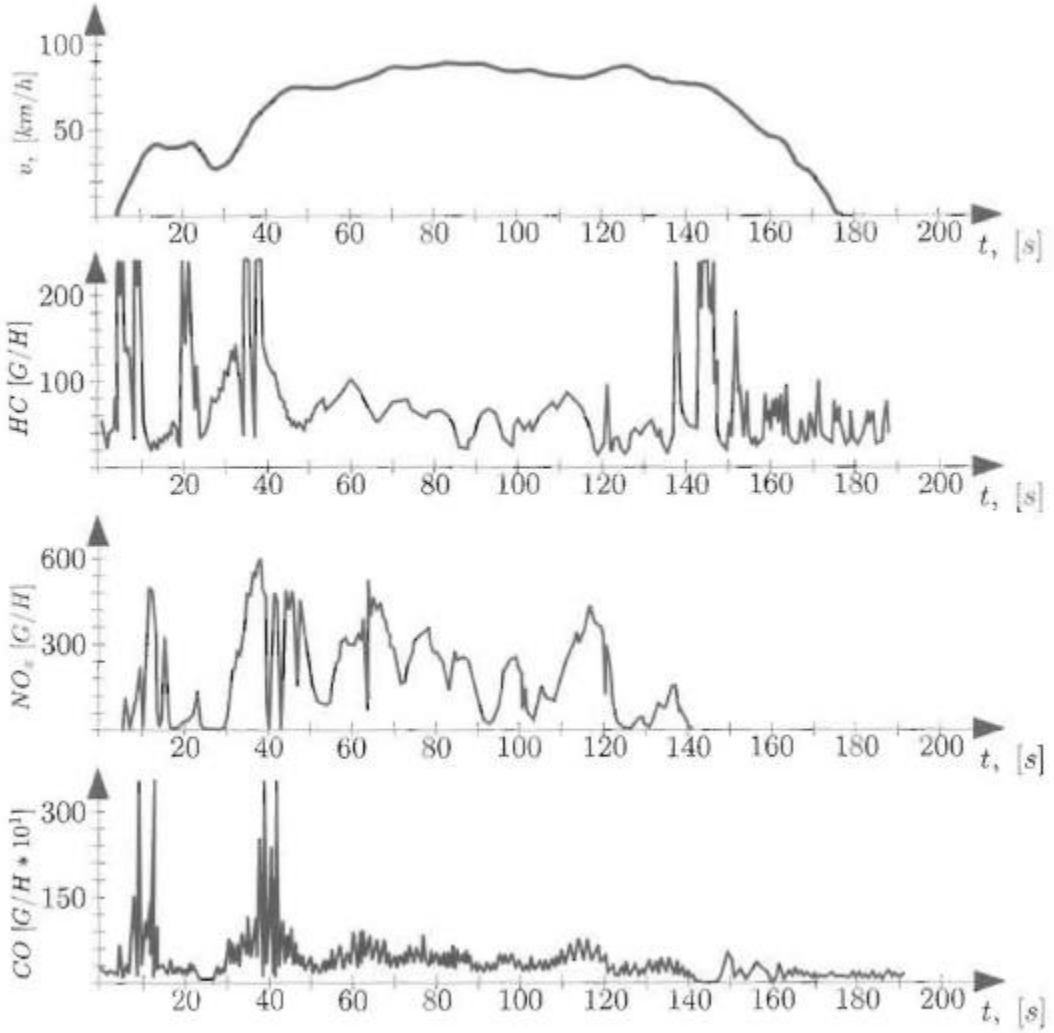

Figure 4.18 Raw emissions of lambda-controlled engine before catalytic conversion, FTP-HT2 driving-cycle

During this transition time the lambda window is left. In this section the remaining control errors shall be eliminated by an adaptive feed-forward control. By that the original lambda control is relieved from compensating mismatches in transients.

Adaptation of a Feed-forward Control Map

The lambda control loop compensates errors of the air-fuel ratio by a multiplicative correction factor F_λ. These lambda correction factors are stored into a feed-forward control map in all engine operating points. Instead of performing the error compensation by the original lambda control loop, it can now be performed by the right F_λ from the feed-forward control map without time delay. The lambda mismatches during transients are thus overcome.

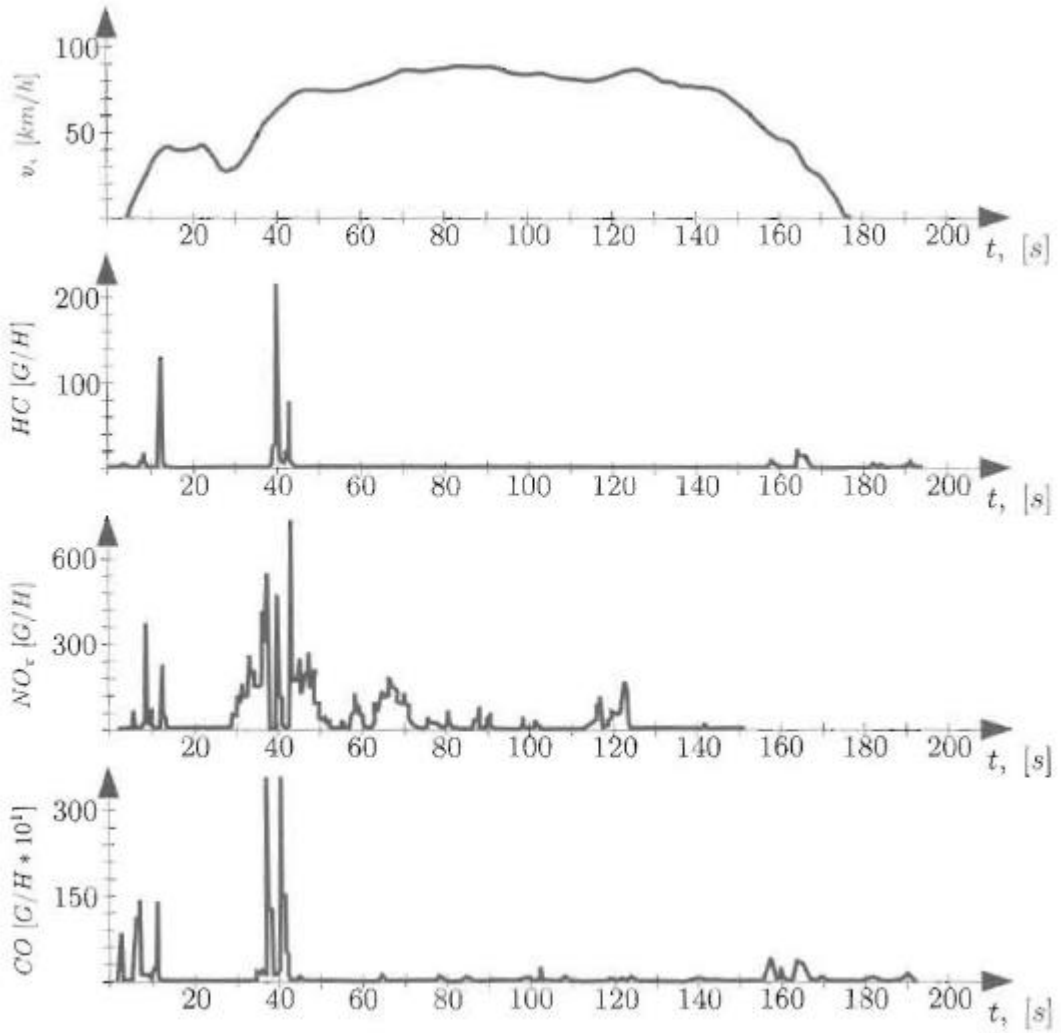

Figure 4.19 Emissions of lambda-controlled engine after catalytic conversion, FTP-HT2 driving-cycle

The problem is how to adapt the correction factors F_λ in the feed-forward control map, when some engine operating points are only very rarely visited, due to special habits of individual drivers. Eventually an adaptation is even impossible. High noxious exhaust emissions would thus remain during transients into these rarely visited operation points. Therefore a globally valid lambda compensation approach is used rather than a local adaptation of correction factors in all engine operating points.

Globally Valid Lambda Compensation

The air-fuel ratio errors are assumed to consist of two components (4.21):

Additive lambda offset error: since the absolute value of this offset is identical over the entire engine operating range, its impact is mostly felt at low

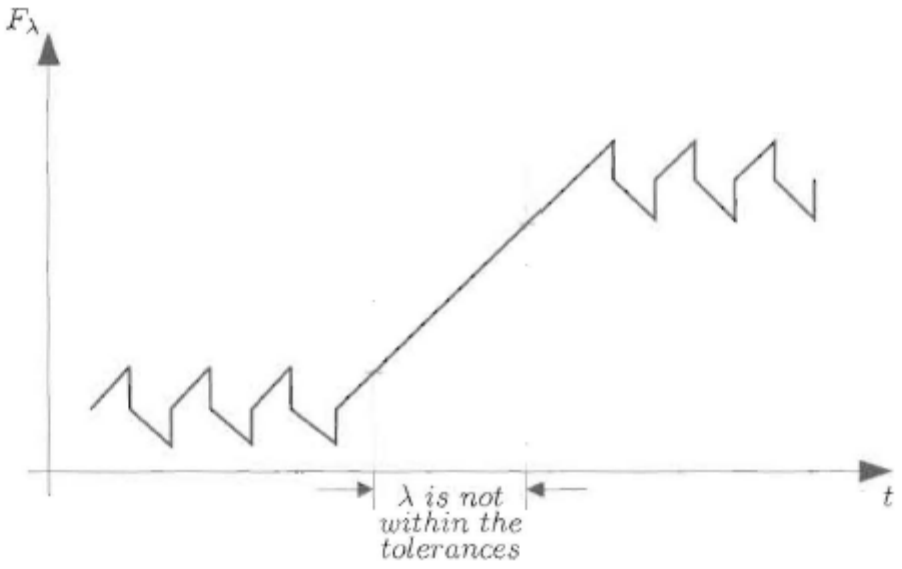

Figure 4.20 Control action F_λ at the transition to a new operating point

engine power outputs. At medium or high power output, the relative error from the offset may be neglected. An example is air leakage bypassing the mass air flow meter.

Multiplicative lambda errors: since the gradient of the linear lambda function between fuel and air mass flow is affected, its impact is equally felt at any engine operation. An example is the air density error at flap type air flow meters.

This simplified error model is supported by practical experience in engine management systems.

The additive and multiplicative errors shall now be compensated. The correct air mass flow would have been

$$\dot{m}_{a,o} = \lambda_0 L_{St} \dot{m}_f \quad . \tag{4.31}$$

The corrupted characteristic is then

$$\begin{aligned} \dot{m}_a &= \lambda L_{St} \dot{m}_f + \Delta \dot{m}_a \\ &= \frac{\lambda}{\lambda_0} \dot{m}_{a,0} + \Delta \dot{m}_a \quad . \end{aligned} \tag{4.32}$$

The compensation scheme comprises two steps.

a.) At **medium** and **high** engine power outputs, the additive error can be neglected.

$$\frac{\dot{m}_a}{\dot{m}_{a,0}} = \frac{\lambda}{\lambda_0} + \underbrace{\frac{\Delta \dot{m}_a}{\dot{m}_{a,0}}}_{\approx 0} \approx \frac{\lambda}{\lambda_0} \tag{4.33}$$

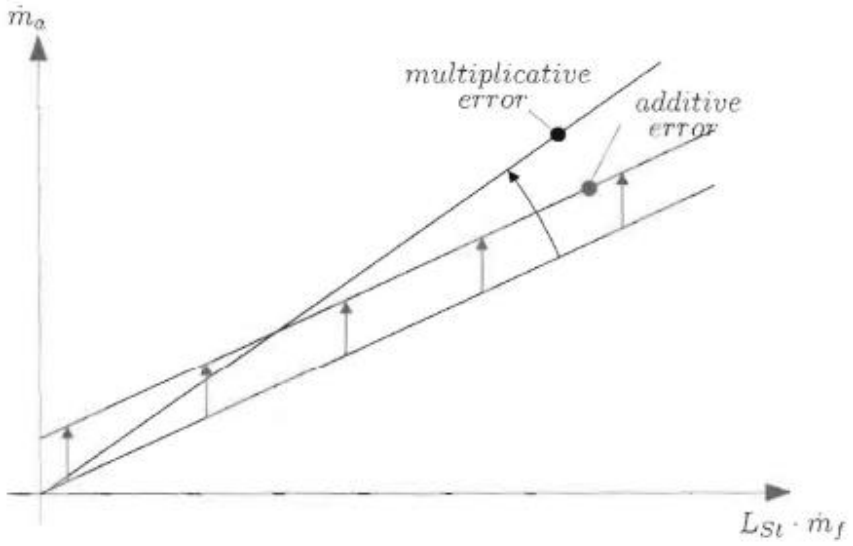

Figure 4.21 Simplified error model for the lambda characteristic

The remaining multiplicative lambda error can then be compensated by the regular lambda control loop which generates a control output factor F_λ inversely proportional to $\frac{\lambda}{\lambda_0}$. It is averaged to suppress the limit cycle.

$$\overline{F}_\lambda = \frac{\lambda_0}{\lambda} \tag{4.34}$$

In the absence of errors, $F_{\lambda 0}$ would have been equal to 1 (stochiometric). The product

$$\overline{F}_\lambda \cdot \frac{\dot{m}_a}{\dot{m}_{a,0}} \approx 1 \tag{4.35}$$

recovers the uncorrupted air-fuel ratio. The control output is low-pass filtered into $\overline{F}_\lambda$ and is stored in a non-volatile memory at medium and high engine power outputs.

$$F_{Hi} = \overline{F}_\lambda \tag{4.36}$$

Taking advantage of the compensation factor F_{Hi}, the corrected mass air flow $\dot{m}_{a,0}$ can be calculated from the measured one $\dot{m}_a$.

$$F_{Hi} \cdot \dot{m}_a \approx \dot{m}_{a,0} \tag{4.37}$$

By application of F_{Hi}, the gradient of the lambda characteristic is turned back to λ_0.

b.) This is now employed at low engine power outputs. The additive offset error $\Delta\dot{m}_a$ can no longer be neglected.

$$\dot{m}_a = \frac{\lambda}{\lambda_0}\dot{m}_{a,0} + \Delta\dot{m}_a \tag{4.38}$$